Polymer Bulletin 53, 213–222 (2005)
DOI 10.1007/s00289-004-0329-2

Polymer Bulletin

Grazing Incidence X-ray Diffraction Study on Surface Crystal Structure of Polyethylene Thin Films

Hirohiko Yakabe[1], Keiji Tanaka[1], Toshihiko Nagamura[1], Sono Sasaki[2], Osami Sakata[2], Atsushi Takahara[3] and Tisato Kajiyama[4] (✉)

[1]Department of Applied Chemistry, Faculty of Engineering, Kyushu University, Fukuoka 812-8581, Japan
[2]Japan Synchrotron Radiation Research Institute, Mikazuki, Sayo, Hyogo 679-5198, Japan
[3]Institute for Materials Chemistry and Engineering, Kyushu University, Fukuoka 812-8581, Japan
[4]Kyushu University, Fukuoka 812-8581, Japan
E-mail: kajiyama@cstf.kyushu-u.ac.jp, Fax: +81-92-651-5606

Received: 13 October 2004 / Revised version: 2 December 2004 / Accepted: 14 December 2004
Published online: 7 January 2005

Summary

Crystal structure in thin films of melt-crystallized and annealed polyethylene (PE) was examined by grazing incidence X-ray diffraction measurements. Choosing appropriate incident angles of X-rays to the films, surface and bulk molecular aggregation states were successfully extracted. Consequently, it was found that chain packing structure in the surface region was different from that in the bulk one. Based on paracrystalline analysis for the (110) reflection and its higher-order ones of PE orthorhombic crystal, it was clarified that the ordering for the crystalline lattice was lower in the surface region. Also, apparent crystallinity in the surface was lower than the bulk one. These results indicate that disordered crystallites were preferentially formed in the surface region.

Introduction

Surface structure and physical properties of polymeric materials have been received a great deal of attention because they should be strongly correlated to the manifestation of functionality at the surface [1]. Considering mass consumption of polymers in the industrial field, crystalline polyolefin can be regarded as a class of most consumed polymers due to its excellent cost performance [2]. Hence, understanding structure and physical properties at the surface of crystalline polyolefin is crucial so that future functional materials with an excellent cost performance will be designed and constructed. So far, surface morphology of typical crystalline polyolefin has been extensively explored by many research groups with the advent of modern microscopic techniques [3-6]. In addition, surface sensitive spectroscopic measurements have also been applied to films of crystalline polyolefin, leading a finding that short-range conformation at the film surface was not the same as that in the corresponding bulk phase [7-9]. However, for the moment, a little information has been known on how surface crystalline structure differs from the bulk one for polyolefin.

A technique of grazing incidence X-ray diffraction (GIXD) [10] enables us to gain direct access to information upon crystalline structure at the film surface by choosing an appropriate condition. Up to date, GIXD has revealed crystalline structure at the film surface of polyimide [11,12], poly(pyromellitic dianhydride-oxydianiline) [13], isotactic polypropylene [14-16], and poly(ethylene terephthalate) [17]. However, to the best of our knowledge, detail molecular aggregation states at the film surface of high-density polyethylene (HDPE), which is the most typical and simple crystalline polymer, are open to study yet. Although surface crystalline structure of various polymers should be clarified one by one, the most important and intriguing point is to establish universality of why crystalline structure at the surface is supposed to be different from that in the bulk. In that sense, a polymer with simplest chemical structure should be used.

The objective of this study is to clarify the lattice dimension and distortion in the surface region of HDPE films by GIXD measurements. Since our goal is to understand characteristics of pristine polymer surface, we strictly restrict ourselves to not use compression-molded samples, although it is better to be used in terms of surface roughness. Hence, the HDPE films prepared by a dip-coating method are used. And, crystalline structure generally depends on how the film was prepared. Thus, two kinds of HDPE films, annealed and melt-crystallized, are examined in this study.

Experimental

As a material, additive free HDPE (Melt Index = 14) was kindly supplied from Mitsui Chemicals, Inc. The melting point (T_m) of HDPE was evaluated to be 404 K by differential scanning calorimetry under dry N_2 purge at the heating rate of 10 K•min^{-1}. Thin films of HDPE were prepared onto silicon wafers with a native oxide layer by a dip-coating method from a 1.0 wt% *p*-xylene solution under N_2 atmosphere. The substrates were dipped into the solution heated at 373 K for 5 min, and were pulled out at the rate of 25 mm•sec^{-1}. Thickness of the films obtained was approximately 400 nm. Then, two different treatments were made on the thin films, resulting in two different films such as annealed films and melt-crystallized ones. For the annealing treatment, the as-prepared thin films were simply placed on a hot stage at various temperatures (T_a) for 24 h under N_2 atmosphere. Besides, for the melt-crystallized thin films, as-prepared thin films were firstly melted on a hot stage at 443 K for 10 min under N_2 atmosphere, and then, were isothermally kept at various crystallization temperatures (T_c) for 24 h. Atomic force microscopic observation has revealed that spherulitic structure was formed in all HDPE films. The root-mean-square roughness of the films was approximately 10 nm.

Crystalline structure in the HDPE thin films was examined by GIXD measurements. The measurements were carried out at the BL-13XU beamline [18] of SPring-8 at Japan Synchrotron Radiation Research Institute. The wavelength (λ) of monochromatized incident X-rays used was 0.128 nm. The size at incident slits was 0.10 and 0.06 mm in the normal and parallel directions to the ground, respectively. And a soller slit was placed before scintillation counter. The data collection time was 3 s per a step, and the angular interval was 0.05º. To prevent the HDPE thin films from surface oxidation, a sample cell purged with He gas was used. In addition, aluminum attenuators were installed in front of a sample to optimize the incident beam intensity. Microscopic infrared spectroscopy confirmed that the sample after the measurements was not oxidized. Figure 1 shows the schematic geometries of (a) in-

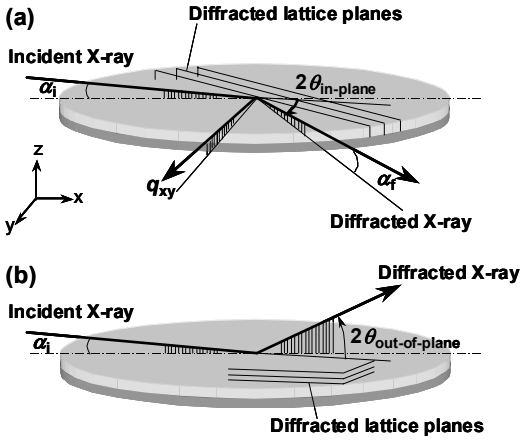

Figure 1. Schematic geometries of (a) in-plane and (b) out-of-plane GIXD measurements.

plane and (b) out-of-plane GIXD measurements. When the incident angle (α_i) of X-rays to the sample surface is equal to, or smaller than, the critical angle (α_c), the incident X-rays undergo total external reflection and penetrate into the sample as evanescent waves. The penetration depth (d_p) of evanescent waves is defined as a depth, at which the intensity decreases to be e^{-1}, and is expressed by

$$d_p = \frac{1}{\sqrt{2}k\left\{\sqrt{\left(\alpha_c^{\,2} - \alpha_i^{\,2}\right)^2 + 4\beta^2} + \alpha_c^{\,2} - \alpha_i^{\,2}\right\}^{1/2}} \qquad (1)$$

where k is wave vector and β is defined as $\mu\lambda/4\pi$, and μ is linear absorption coefficient. And, the α_c value is given by

$$\alpha_c = \left(\frac{\lambda^2 r_e N}{\pi}\right)^{1/2} \qquad (2)$$

where r_e is classical electron radius and N is electron density per unit volume of materials. For our experimental condition with λ = 0.128 nm, the α_c is calculated to be 0.125º. Thus, we chose the α_i values of 0.11 and 0.20º for the surface- and bulk-sensitive measurements. Invoking that the sample surface of the HDPE films is infinitely flat, the ideal penetration depth of X-rays is supposed to be 9.6 nm for α_i = 0.11º. Reflection from crystalline planes in the samples was detected with a scintillation counter scanned in the in-plane and out-of-plane directions. In the in-plane geometry, scattering vector (q) is parallel to the surface, and thus, the detected profiles reflect information upon crystalline structure normal to the sample surface. On the other hand, information about the structure parallel to the surface is obtained from the out-of-plane geometry. In this case, a peak position obtained experimentally should be corrected because it was slightly shifted from the corresponding Bragg angle due to refraction of incident X-rays at the sample surface. The value of this shift ($\Delta 2\theta$) is expressed by [19]

$$\Delta 2\theta = \alpha_i - \frac{1}{\sqrt{2}}\left\{\left[\left(\alpha_i^2 - \alpha_c^2\right)^2 + 4\beta^2\right]^{1/2} - \alpha_c^2 + \alpha_i^2\right\}^{1/2} \quad (3)$$

From this equation, the $\Delta 2\theta$ values for α_i = 0.11 and 0.20º were 0.110 and 0.046º, respectively.

Results and discussion

Melt-crystallized HDPE thin films

Figure 2 shows (a) in-plane and (b) out-of-plane GIXD profiles for a melt-crystallized HDPE thin film measured at α_i = 0.11 and 0.20º. As a typical example, the profiles for the film isothermally crystallized at 378 K from the melt are displayed. The profiles measured at α_i = 0.11 and 0.20º reflect the crystal structure in surface and bulk regions, respectively. The scattering vector (q) was defined as $(4\pi/\lambda)\bullet\sin\theta$. Overlapping peaks were separated using a least-square fitting procedure. Based on reflection peaks observed, it is clear that the orthorhombic crystal structure was formed in the films. Interestingly, the in-plane GIXD profiles were quite different from the out-of-plane ones. In the case of the in-plane geometry, the intensity of the (020) reflection was much stronger than that of the (200) reflection. On the other hand, only the (200) reflection was observed in the q range employed for the out-of-plane geometry. These results indicate that the a and b axes of an orthorhombic unit cell preferentially oriented normal and parallel to the film surface, respectively. Also, the intensities of (110) and (200) reflections by the in-plane measurements were invariant with respect to the rotational angle of the film around the normal axis to the surface, namely, azimuthal angle, meaning that the film was crystallographically isotropic in the lateral direction. Since the crystallographic b axis of the PE orthorhombic unit cell is generally parallel to the spherulitic radius [20], it seems most likely that lamellar crystals would grow two-dimensionally in the parallel direction to the film surface.

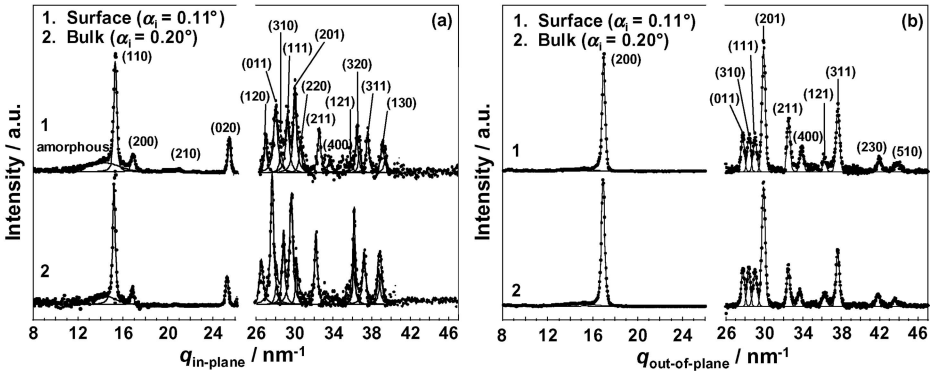

Figure 2. (a) in-plane and (b) out-of-plane GIXD profiles for melt-crystallized HDPE thin film measured at α_i = 0.11 and 0.20°. The profiles are for the film isothermally crystallized at 378 K from the melt.

We now turn to lattice dimension and distortion in the surface region of the HDPE thin films. Figure 3 shows the T_c dependences of lattice constants *a, b* and *c* for the PE orthorhombic unit cell in the surface and bulk regions. The lattice constants were determined on the basis of the *q* values, at which the corresponding reflections were observed. In all T_c range examined, the *a* and *b* axes in the surface were shorter than those in the internal bulk phase. This would be interpreted by taking into account a notion that molecular packing state such as a setting angle differs in surface and bulk regions. The setting angle, which is defined as an angle between the polymer zigzag chain and the *b* axis of the unit cell, is dependent on internal strain and/or lamellar thickness [21]. Since the HDPE films employed were quite thin, the crystal structure would be affected by the substrate. Taking into account that the thermal expansion coefficient for HDPE is larger than that for silicon substrate by approximately 40 times [22,23], it is plausible that crystalline lattice in the bulk region might be distorted due to the thermal expansion difference between the two upon melt-crystallization. On the other hand, in the surface region, the crystalline phase with a larger distortion or strain was in part transformed to a paracrystal state, which is defined as a model of disorder in crystalline system, during the isothermal crystallization process so that the internal strain in crystalline lattice could be released. In other words, only crystal lattice with a relatively smaller internal strain is remained in the surface region. Hence, the lattice constants *a* and *b* in the surface region became smaller than the corresponding bulk values. And, the *a* and *b* monotonically increased with increasing T_c in both regions but the *c* remained to be constant within our experimental accuracy. Thus, it can be envisaged that the crystallographic *c* axis of the PE orthorhombic unit cell was dimensionally stable to T_c because it was parallel to the chain axis. Also, the relation of the *a* and *b* values to temperature implies that the internal strain due to thin film increased with increasing T_c in both surface and bulk regions.

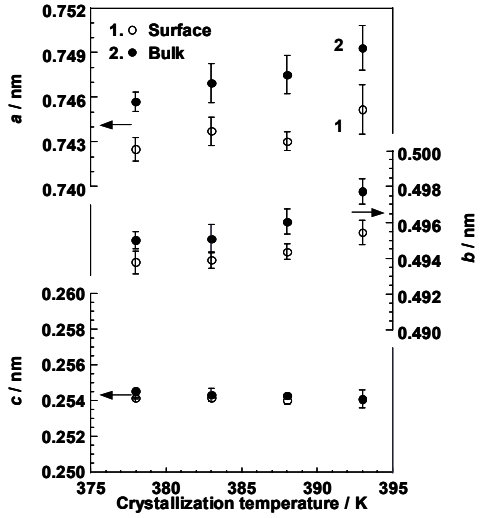

Figure 3. Crystallization temperature dependences of the lattice constants *a, b* and *c* for the PE orthorhombic unit cell in the surface and bulk regions. Open and closed figures denote surface and bulk regions, respectively.

For the GIXD measurement, an effect of surface roughness should be considered. When the sample surface possesses a finite roughness, incident X-rays might penetrate into the bulk region even under the condition of $\alpha_i < \alpha_c$, depending on to what extent the surface roughness is. If the surface roughness is quite large and thus X-rays deeply penetrate into the internal region, the measurement is not suitable as a surface sensitive characterization method. However, in our experiment, crystalline structure in the surface region was discerned to be markedly different from that in the corresponding internal phase. Thus, we are convinced that the measurement is still powerful for the analysis of crystalline structure in the surface region with the 10 nm-roughness.

We next try to extract how the crystal lattice is distorted in the in-plane direction on the basis of the paracrystalline analysis [24] using higher order reflections. Such an analysis can be only attained by a strong light source of X-rays. In the paracrystalline lattice model, the lattice vectors of adjacent unit cells vary in magnitude and direction due to large displacement of lattice points from their ideal positions, which results in a loss of the long-range crystallographic order. Assuming that the coordination statistics distribution function for the paracrystalline lattice model is in the form of Gaussian distribution, paracrystalline lattice factor [$Z(s)$] of the h-th order reflection is defined as

$$Z(s) = Z(h) = \frac{1 - \exp(-4\pi^2 g^2 h^2)}{\left[1 - \exp(-2\pi^2 g^2 h^2)\right]^2 + (4\sin^2 2\pi h)\exp(-2\pi^2 g^2 h^2)} \qquad (4)$$

where s is reciprocal lattice vector, h is scattering order and g is standard deviation of the Gaussian distribution divided by average lattice vector ($\tilde{a}$). Thus, the g value is fluctuation in the lattice vector as a parameter to evaluate the degree of paracrystalline lattice distortion. As a crystal lattice becomes disordered from an ideal one, the g becomes larger. The value of g is experimentally given by

$$(\delta\beta)^2 = \frac{\frac{1}{N^2} + \pi^4 g^4 h^4}{\tilde{a}^2} \qquad (5)$$

Here, $\delta\beta$ is integral width of Gaussian peaks fitted to reflections and N is number of scattering units, which reflects crystallite size. Since the relation between $(\delta\beta)^2$ and h^4 was linear, the g and N for the (110) were calculated by intercept and slope of the line using equation 5. Basically, g and N values were estimated using (110), (220) and (330) reflections. However, the (330) reflection was not clearly observed for some samples, as seen in Figure 2. When the (110), (220) and (330) reflection peaks were observed, the g and N values were tried to be calculated only by two data sets from (110) and (220) reflections. Interestingly, the g and N values so obtained were in good accordance with those based on the three reflection peaks. Hence, when the higher order reflection was not observed, the g and N values were calculated by the two points. Figure 4 shows the T_c dependences of (a) $g_{(110)}$ and (b) $N_{(110)}$ in the surface and bulk regions for the HDPE thin films, respectively. As shown in the part (a), the surface $g_{(110)}$ was larger than the bulk one at a given temperature, indicating that the paracrystalline lattice distortion of the orthorhombic unit cell would be larger in the surface region than in the bulk region. On the other hand, the difference of $N_{(110)}$ between surface and bulk was trivial. This means that crystallite size in the in-plane

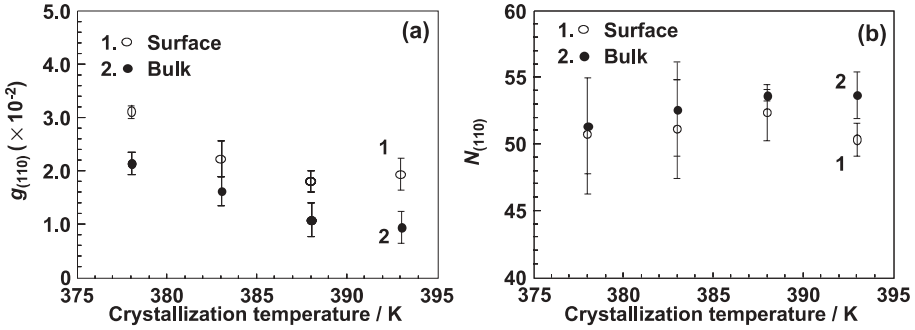

Figure 4. Crystallization temperature dependences of the (a) $g_{(110)}$ and (b) $N_{(110)}$ in the surface and bulk regions for the HDPE thin films. Open and closed figures denote surface and bulk regions, respectively.

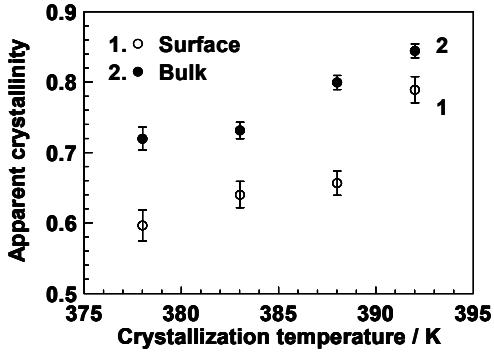

Figure 5. Crystallization temperature dependences of apparent crystallinity in the surface and bulk regions for the HDPE thin films. Open and closed figures denote surface and bulk regions, respectively.

direction would be uniform in the films. Figure 5 shows the T_c dependences of apparent crystallinity in the surface and bulk regions. In the case of the in-plane measurements, only crystalline lattice planes normal to the sample surface were detected. This means that the crystallinity obtained does not necessarily correspond to the value for the crystals randomly oriented. Hence, the term of apparent crystallinity is used in this study. The value in the surface region was lower than that in the bulk at a given temperature. And, the apparent crystallinity in both regions increased with increasing T_c. As shown in Figure 4, the $g_{(110)}$ value in the surface region was higher than the corresponding bulk value, implying that paracrystal is preferentially existed in the surface region. Since the dissipation of latent heat should be more remarkable near the surface, imperfect crystallization of chains proceeded in the surface region, resulting in the formation of paracrystal. Or otherwise, the preferential formation of paracrystal in the surface region would be understood on the basis of chain mobility. The chains near the surface are more mobile than those in the interior bulk region. Thus, upon isothermal crystallization, crystal lattice with a larger internal strain transforms to paracrystal phase to release the internal strain in the surface region, although this is almost not the case in the bulk. For the moment, it can be hardly judged which factor was dominant for the preferential formation of the paracrystal state at the surface in the HDPE film.

Annealed HDPE thin films

An annealing effect on crystal structure in the HDPE thin films is discussed. Figure 6 shows annealing temperature dependences of lattice constants *a*, *b* and *c* in both surface and bulk regions. In the case of the as-prepared film, the lattice constants of *a* and *b* were smaller in the surface than in the bulk, whereas the lattice constant of *c* was almost the same in both regions. These results are essentially similar as for the melt-crystallized films. When the annealing treatment was made on the HDPE films at a temperature higher than 363 K, the *a* and *b* became larger. Such an inclination was more clearly seen in the surface region. Deferring why the crystal lattice became larger at a temperature higher than 363 K, the imperfection of crystal lattice in the in-plane direction was here examined on the basis of the paracrystalline analysis. Figure 7 shows annealing temperature dependences of (a) $g_{(110)}$ and (b) $N_{(110)}$ in the surface and bulk regions of the HDPE thin films. In the case of the as-prepared film, both $g_{(110)}$ and $N_{(110)}$ values in the surface region were larger and smaller than the bulk values, respectively. Hence, it is conceivable that the paracrystal existed more near the surface compared with the interior region of the film, and that the ordering for the crystalline lattice in the surface region was also lower than that in the bulk. Besides, the $g_{(110)}$ and $N_{(110)}$ values changed once the annealing treatment was carried out at a temperature higher than 363 K. This result makes it clear that the amount of the paracrystal decreased and the ordering of crystalline lattice improved upon annealing at temperatures higher than 363 K. Figure 8 shows how apparent crystallinity in the surface and bulk regions of the HDPE films depends on annealing temperature. As a general trend, apparent crystallinity in the surface region was lower than that in the bulk at a given temperature. Since this trend is in good accordance with the relation of $g_{(110)}$ to annealing temperature, as shown in the part (a) of Figure 7, it can be claimed that the paracrystal transformed to the ideal lattice upon annealing at a temperature higher than 363 K.

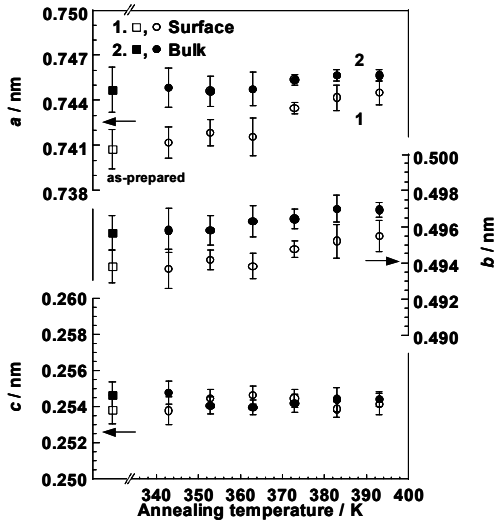

Figure 6. Annealing temperature dependences of the lattice constants *a*, *b* and *c* in the surface and bulk regions of HDPE thin films prepared from the solution at 373 K. Open and closed figures denote surface and bulk regions, respectively. And squared figures show as-prepared film.

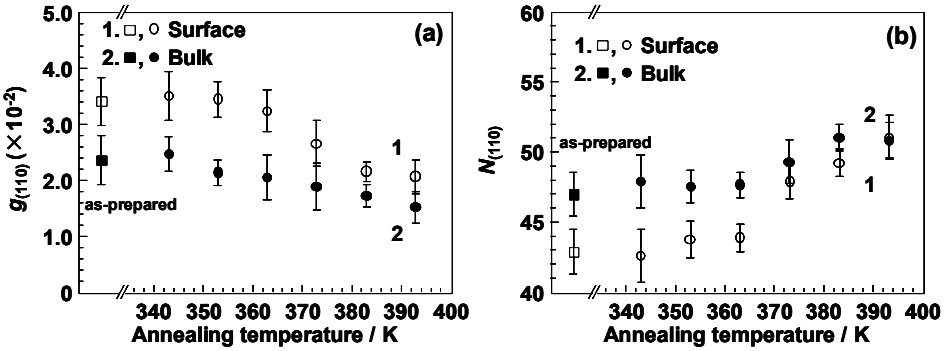

Figure 7. Annealing temperature dependences of (a) $g_{(110)}$ and (b) $N_{(110)}$ in the surface and bulk regions of HDPE thin films prepared from the solution at 373 K. Open and closed figures denote surface and bulk regions, respectively. And squared figures show as-prepared film.

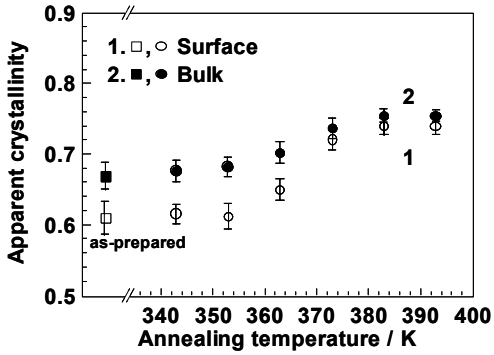

Figure 8. Annealing temperature dependences of apparent crystallinity in the surface and bulk regions of HDPE thin films prepared from the solution at 373 K. Open and closed figures denote surface and bulk regions, respectively. And squared figures show as-prepared film.

For the HDPE films annealed at a temperature lower than 363 K, the lattice constants, the crystalline ordering and the apparent crystallinity were unchanged in comparison with before the annealing. The HDPE films used in this study were prepared from a *p*-xylene solution kept to be 373 K. Thus, a clear annealing effect on crystalline structure was not observed for the HDPE films annealed at a temperature lower than 363 K because of its thermal history. On the other hand, at higher temperatures, especially 383 and 393 K, their difference between surface and bulk became smaller. This result might be understood by taking a notion of enhanced surface mobility [25,26], which enables surface chains to be crystallized.

Conclusions

Crystal structure in the surface and bulk regions of melt-crystallized and annealed HDPE thin films was investigated by GIXD measurements. The dimension of orthorhombic crystal lattice in the in-plane direction was smaller in the surface region than in the bulk region. And the disordering of crystal lattice in the surface region was higher. This tendency was observed despite of preparation in different methods.

Therefore, crystal lattice in the surface region was closely packed and essentially imperfection in comparison with the bulk region.

Acknowledgements. This research was partly supported by Fukuoka Industry, Science & Technology Foundation and the 21st Century COE Project from The Ministry of Education, Culture, Sports, Science and Technology, Japan. The synchrotron radiation X-ray diffraction experiments were performed at SPring-8 with the approval of Japan Synchrotron Radiation Research Institute (JASRI) as Nanotechnology Support Project of The Ministry of Education, Culture, Sports, Science and Technology, Japan.

References

1. Garbassi F, Morra M and Occhiello E (1994) Polymer Surfaces from Physics to Technology, JohnWiley & Sons Ltd, Chichester
2. Galli P and Vecellio G (2001) Prog Polym Sci 26:1287
3. Schonherr H, Snetivy D and Vancso GJ (1993) Polym Bull 30:567
4. Magonov SN and Reneker DH (1997) Annu Rev Mater Sci 27:175
5. Mellbring O, Oiseth KS, Krozer A, Lausmaa J and Hjertberg T (2001) Macromolecules 34:7496
6. Sasaki S, Sakaki Y, Takahara A and Kajiyama T (2002) Polymer 43:3441
7. Hung JB, Hong JW and Urban MW (1992) Polymer 33:5173
8. Kawamoto N, Mori H, Nitta K, Yui N and Terano M (1996) Macromol Chem Phys 197:3523
9. Zhang D, Shen YR and Somorjai GA (1997) Chem Phys Lett 281:394
10. Marra WC, Eisenberger P and Cho AY (1979) J Appl Phys 50:6927
11. Factor BJ, Russell TP and Toney MF (1991) Phys Rev Lett 66:1181
12. Factor BJ, Russell TP and Toney MF (1993) Macromolecules 26:2847
13. Saraf RF, Dimitrakopoulos C, Toney MF and Kowalczyk SP (1996) Langmuir 12:2802
14. Kawamoto N, Mori H, Nitta K, Sasaki S, Yui N and Terano M (1998) Angew Makromol Chem 256:69
15. Kawamoto N, Mori H, Nitta K, Sasaki S, Yui N and Terano M (1998) Macromol Chem Phys 199:261
16. Nishino T, Matsumoto T and Nakamae K (2000) Polym Eng Sci 40:336
17. Durell M, Macdonald JE, Trolley D, Wehrum A, Jukes PC, Jones RAL, Walker CJ and Brown S (2002) Europhys Lett 58:844
18. Sakata O, Furukawa Y, Goto S, Mochizuki T, Uruga T, Takeshita K, Ohashi H, Ohata T, Matsushita T, Takahashi S, Tajiri H, Ishikawa T, Nakamura M, Ito M, Sumitani K, Takahashi T, Shimura T, Saito A and Takahashi M (2003) Surf Rev Lett 10:543
19. Toney MF and Brennan S (1989) Phys Rev B 39:7963
20. Fujiwara Y (1960) J Appl Phys 4:10
21. Phillips PJ and Tseng HT (1985) Polymer 26:650
22. Brandrup J, Immergut EH and Grulke EA (1999) Polymer Handbook, 4th ed., JohnWiley & Sons Ltd, New York
23. Weast RC (1987) CRC Handbook of Chemistry and Physics, 68th ed., CRC Press Inc, Florida
24. Lindenmeyer PH and Hosemann R (1963) J Appl Phys 34:42
25. Takana K, Takahara A and Kajiyama T (2000) Macromolecules 33:7588
26. Kawaguchi D, Tanaka K, Kajiyama T, Takahara A and Tasaki S (2003) Macromolecules 36:1235